ACS Energy LETTERS

http://pubs.acs.org/journal/aelccp

LETTER

Photovoltage Tomography in Polycrystalline Solar Cells

Elizabeth M. Tennyson,[†,‡] Jesse A. Frantz,[§] John M. Howard,[†,‡] William B. Gunnarsson,[‡,∥] Jason D. Myers,[§] Robel Y. Bekele,[⊥] Jasbinder S. Sanghera,[§] Suok-Min Na,[#] and Marina S. Leite*[,†,‡]

[†]Department of Materials Science and Engineering, [‡]Institute for Research in Electronics and Applied Physics, [∥]Department of Electrical and Computer Engineering, and [#]Department of Aerospace Engineering, University of Maryland, College Park, Maryland 20742, United States

[§]U.S. Naval Research Laboratory, Washington, D.C. 20375, United States

[⊥]University Research Foundation, Greenbelt, Maryland 20770, United States

Supporting Information

ABSTRACT: To date, the performance of all polycrystalline photovoltaics is limited by their open-circuit voltage (V_{oc}), an indicator of charge carrier recombination within the semiconductor layer. Thus, the successful implementation of high-efficiency and low-cost solar cells requires the control and suppression of nonradiative recombination centers within the material. Here, we spectrally and spatially resolve the photovoltage of polycrystalline thin-film Cu(In,Ga)Se_2 (CIGS) solar cells. Micro-Raman and energy-dispersive X-ray spectroscopy maps obtained on the same grains showed that the chemical composition of the CIGS layer is very uniform. Surprisingly, we observed concurrent spatial variations in the photovoltage generated across the device, strongly indicating that structural properties are likely responsible for the nonuniform mesoscale behavior reported here. We build a tomography of the photovoltage response at 1 sun global illumination, mimicking the operation conditions of solar cells. Furthermore, we spatially resolve the voltage within the CIGS grains, where we found variations >20%. Our functional characterization could be realized to identify where nonradiative recombination preferentially takes place, enabling the implementation of nonuniform materials for future devices with higher V_{oc}.

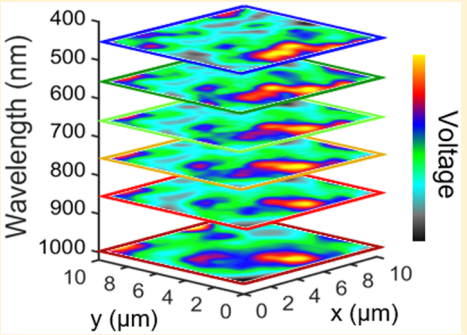

Thin-film polycrystalline solar cells, such as Cu(In,Ga)Se_2 (CIGS), are a practical alternative to commercially available Si photovoltaic (PV) devices because of their low cost and high efficiency.[1,2] Furthermore, these technologies have the advantage of being fabricated on top of either a rigid or flexible substrate, extending solar cell devices toward a variety of applications. To date, the record CIGS device has an impressive efficiency of η = 21.7% and open-circuit voltage of V_{oc} = 748 mV, which was fabricated using the well-established multistage coevaporation technique.[3,4] However, the sequential deposition steps substantially increase the overall production cost of CIGS, preventing its wide commercialization.[5,6] An alternative fabrication technique is the sputter deposition of CIGS through a single quaternary target.[7−9] This method can be implemented in large-scale applications and also avoids a necessary but toxic postdeposition selenization step.[10] Despite the advantages of the quaternary target method, the typical open-circuit voltage (V_{oc}) of the PV devices is ∼500 mV, well below the Shockley−Queisser theoretical limit (∼813 mV for CIGS with E_g = 1.213 eV).[11,12] Thus, the V_{oc} currently restricts the performance of CIGS solar cells. Because the CIGS absorbing layer is inhomogeneous and composed of microscale grains, it has been speculated that the electrical response of the material could be limited either by composition variations within the grains or by the different interfaces throughout the thin-film polycrystalline layer.[13,14]

To probe the local structural and electrical characteristics of materials for PV, scanning probe and electron microscopies have been widely implemented.[13,15,16,31] The local electrical response of these inhomogeneous materials have been determined by laser-beam[17−22] and electron-beam induced current (EBIC),[23−26] conductive-atomic force microscopy,[27−30] Kelvin probe force microscopy (KPFM),[27,31,32] scanning probe microwave capacitance,[33] near-field scanning optical microscopy,[17,18,34−36] cathodoluminescence,[37,38] and photoluminescence.[39−44] Furthermore, spectroscopic methods, including electron energy loss spectroscopy (EELS)[45] and X-ray microscopy,[46,47] have been implemented to reveal how

Received: August 4, 2016
Accepted: September 27, 2016

DOI: 10.1021/acsenergylett.6b00331
ACS Energy Lett. 2016, 1, 899−905

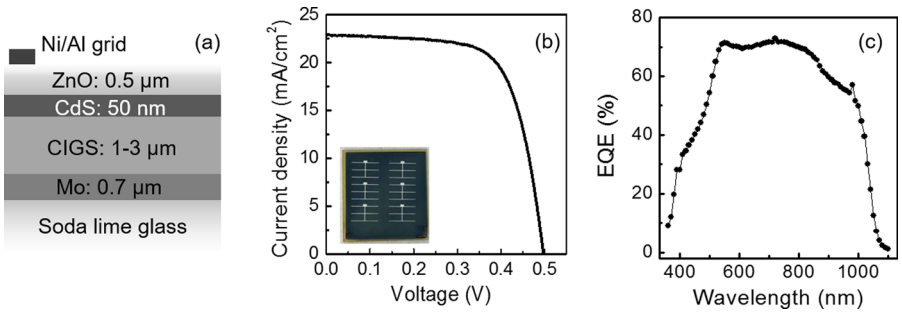

Figure 1. CIGS polycrystalline solar cells fabricated by sputter deposition from a quaternary target. (a) Schematic of CIGS solar cell, out of scale for clarity. (b) Representative light $I-V$ curve for device illuminated with AM1.5G at 1 sun, yielding V_{oc} = 490 mV and η = 7.77%. The inset shows a photograph of six solar cells electrically isolated on a single 1 in. × 1 in. glass substrate. (c) EQE measurement of the same device shown in panel b.

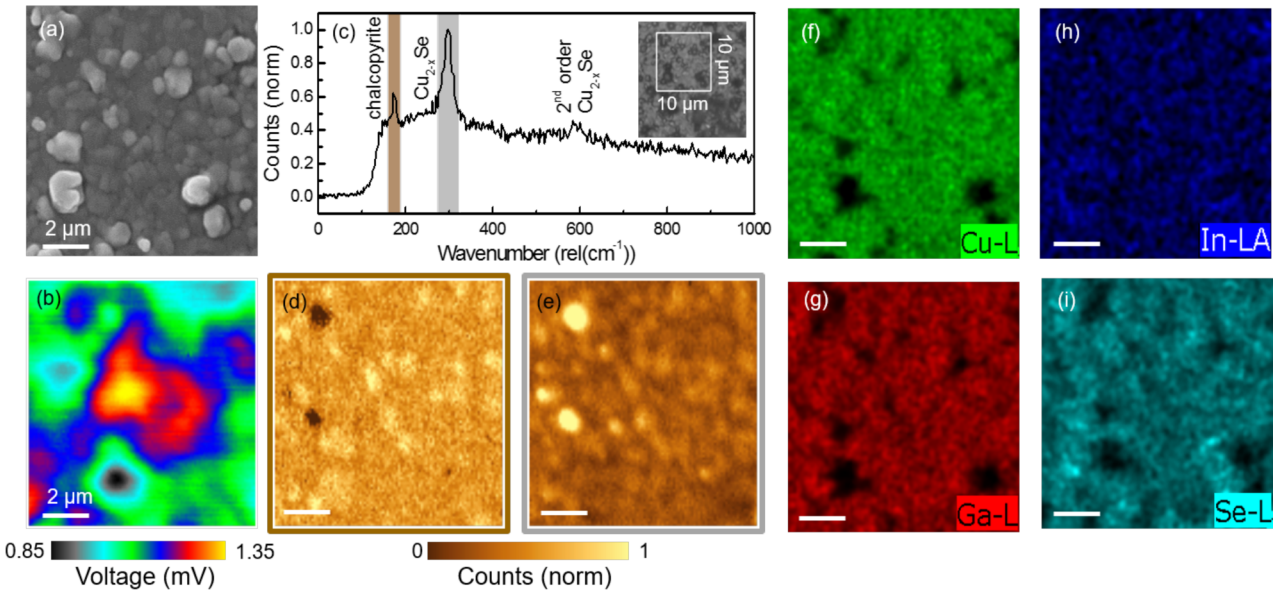

Figure 2. Chemical composition and local electrical response of CIGS solar cells. (a) SEM image of CIGS. (b) Photovoltage map showing spatial variation >15%; illumination conditions: 100× objective, λ = 575 ± 3 nm, and incident power = 298 ± 3 μW. (c) Representative Raman spectrum. Inset: optical micrograph indicating the region where EDX, photovoltage, and Raman measurements were acquired (white box). Raman maps of (d) $Cu_{2-x}Se$ peak (gray filter in panel c) and (e) chalcopyrite peak (brown filter in panel c). Illumination conditions for Raman: λ = 532 nm and incident power = 100 ± 5 μW. EDX maps showing (f) Cu, (g) Ga, (h) In, and (i) Se uniform distribution.

chemical composition variations within the active layers affect the electrical response of the devices. Recently, micro-Raman mapping also became a tool to link material composition to optoelectronic properties.[48,49] Nevertheless, a high spatial resolution (<1 μm) spectroscopic imaging plaform to resolve possible photovoltage variations of polycrystalline solar cells that does not require special sample preparation or an inert environment is still missing.

Here, we spectrally and spatially resolved the photovoltage of polycrystalline thin-film CIGS solar cells from a quaternary target, which is related to the charge carrier recombination events within the absorbing layer of the device. Micro-Raman maps obtained on the *same* grains revealed that the chemical composition of the CIGS layer is very uniform, in agreement with our energy-dispersive X-ray spectroscopy (EDX) results. Surprisingly, we observed concurrent spatial variations in the photovoltage generated across the device, strongly indicating that structural properties are likely responsible for the nonuniform mesoscale behavior reported here. We built a qualitative tomography of the photovoltage through a sequence of spectrally dependent voltage scans at low photon injection level, mimicking realistic operation conditions of photovoltaic devices. The mesoscale electrical response of the material varied at the same length scale as the grains, and different sites (interfaces and groups of grains) showed distinct photovoltage, depending on wavelength, where voltage variations >20% were measured. Our results demonstrate that the V_{oc} of CIGS solar cells is limited by the types of interfaces existing between the grains composing the active layer of the devices. Furthermore, we provide a universal and direct method to map voltage with high spatial resolution without the use of a scanning probe or vacuum environment that can be applied to other optoelectronic devices, such as LEDs, photodetectors, etc.

We utilize standard characterization methods to obtain the macroscopic photovoltaic performance of the CIGS solar cells investigated here. Figure 1a displays a schematic of the CIGS solar cells fabricated via sputtering from a single quaternary target; the details concerning the device fabrication are described in the Supporting Information and in ref 7. The light $I-V$ curve obtained under standard 1 sun AM1.5 G illumination and the external quantum efficiency (EQE) are shown in Figure 1b,c. The inset is a photograph of six

DOI: 10.1021/acsenergylett.6b00331
ACS Energy Lett. 2016, 1, 899−905

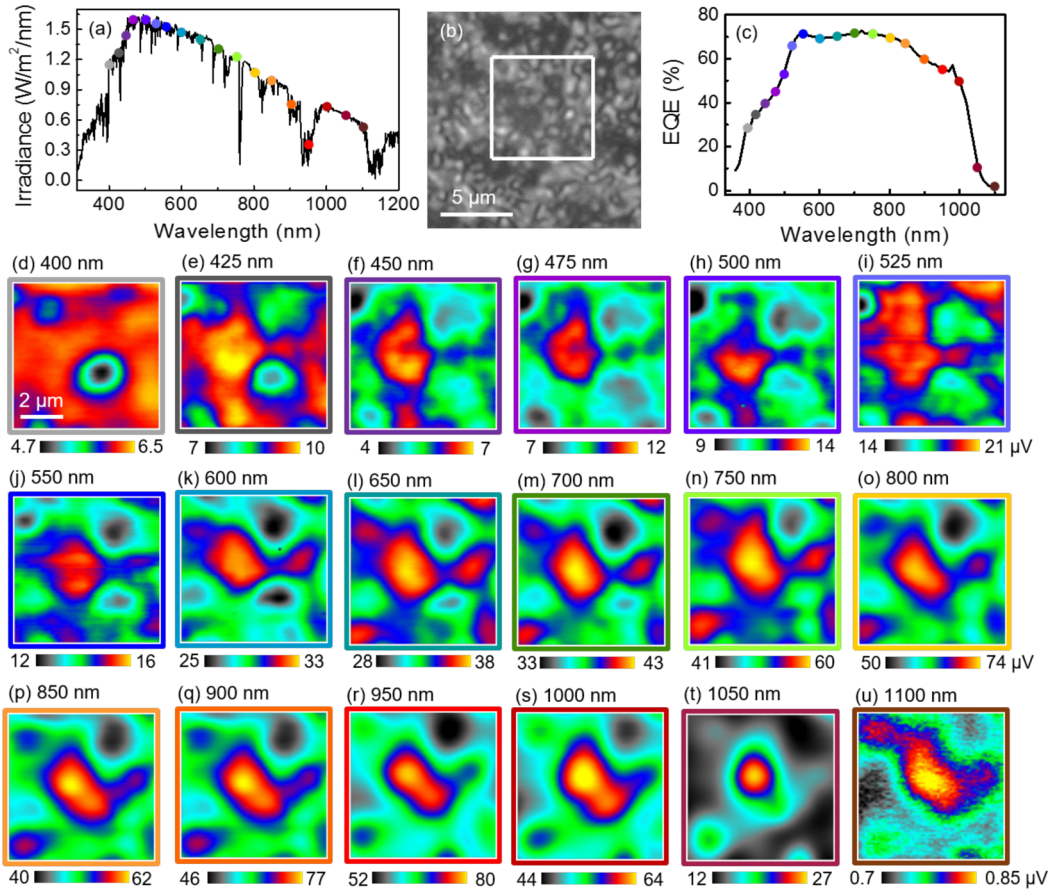

Figure 3. Spectrally dependent voltage maps on CIGS solar cell. (a) One sun AM1.5G spectrum as a function of wavelength. (b) Optical micrograph of CIGS solar cell acquired with 100× objective, NA = 0.75, spot size ~1 μm. The white box highlights the 7 × 7 μm^2 area where the photovoltage measurements were performed. (c) EQE measurement. The colored dots in panels a and c represent the wavelengths of photovoltage scans. (d–u) Spectrally dependent scanning photovoltage microscopy. For each scan, the label indicates the wavelength, and the color scale bar is in microvolts.

electrically isolated CIGS devices on a single 1 in. × 1 in. glass substrate. The low EQE for wavelengths <500 nm results from the expected light absorption by the ZnO (with $E_g \cong 3.3$ eV) layer and the CdS *n*-layer (with $E_g = 2.4$ eV).[50]

We investigate the relationship between the chemical composition and the electrical properties of the CIGS devices by micro-Raman imaging and EDX in conjunction with scanning photovoltage microscopy on the same grains. Figure 2a shows a representative SEM image of the CIGS layer, composed of grains ~1 μm in size, preferentially orientated along the ⟨112⟩ direction (see Figure S1 for an electron backscatter diffraction (EBSD) map). For the scanning photovoltage measurements, a 100× objective lens is used to focus the local source of excitation. A schematic of the experimental setup, photovoltage scans of multiple regions, and a test measurement can be found in Figures S2–S4. We measure remarkable spatial variations in the photovoltage, as shown in Figure 2b. Note that the average voltage signal is small (<2 mV) because of the confined volume of excitation during the measurements (spot area is 0.95 μm^2 compared to the total area of the device, equal to 0.54 cm^2), causing a voltage drop to occur between the dark and light regions of the cell.[51,52] However, the electrical variation in the scanned area is 0.5 mV, considerably higher than the noise (<10 μV). The representative Raman spectrum with both the strong $Cu_{2-x}Se$ and the chalcopyrite peaks is presented in Figure 2c (Raman shifts at 295 and 172 cm^{-1} highlighted in gray and brown, respectively),[53,54] where the inset refers to the optical micrograph of the region mapped. The micro-Raman images corresponding to the $Cu_{2-x}Se$ and chalcopyrite peaks were acquired on the *same* location as the voltage map and exhibit uniform surface chemical composition (despite surface segregation of $Cu_{2-x}Se$); see Figure 2d,e (Figures S5 and S6 present additional Raman maps and SEM image overlaid with the Raman and photovoltage scans). The EDX maps of Cu, Ga, In, and Se presented in Figure 2f–i show very uniform elemental distribution in all cases (within the spatial resolution of the SEM probe used). Our chemical composition measurements strongly indicate that the spatial variation observed in the CIGS electrical response is likely due to the distribution of grain orientation or grain boundary types, which could result in areas of high rates of charge carrier recombination.[23,55]

To understand the contribution of the photovoltage generated within the CIGS grains to the overall performance of the solar cell as a function of light penetration depth, we spectrally resolve the electrical response of the CIGS sample while mimicking the illumination conditions of a working device. See panels a and c of Figure 3 for the 1 sun spectrum at AM1.5G illumination[56] and the EQE, respectively, where the colored dots represent the wavelengths at which the microscopic photovoltage measurements were performed. Figure 3b shows an optical micrograph of the CIGS solar cell. We acquire

DOI: 10.1021/acsenergylett.6b00331
ACS Energy Lett. 2016, 1, 899–905

the photovoltage maps using the same number of incident photons in all cases (Figure 3d−u and Figure S7 for the same voltage scale). The electrical signal continually increases with the wavelength, reaching a maximum value at 950 nm (Figure 3r), approaching the bandgap of the fabricated CIGS layer (equal to 1.15 eV, as determined by photoluminescence). As expected, beyond the semiconductor bandgap (corresponding to wavelength λ > 1000 nm), the electrical signal drops dramatically (Figure 3t,u), indicating that the very modest photogenerated voltage is likely due to trap states within the polycrystalline layer.[17] Nevertheless, spatial variations are still observed and are well above the noise level (20 nV) of the photovoltage measurements introduced here. The *in depth* electrical response of the CIGS layer is obtained without cross-sectioning (destroying) the sample. Although the surface of the sample is being probed, we acquire information about the grains and interfaces due to the absorption coefficient of the material.

The possible contribution of surface roughness and consequent light reflection and scattering to the voltage signal was excluded by a detailed comparison between "as-is" and polished grains, where spatial variations in photovoltage occur irrespective of the morphology of the grains (Figures S8−S10). The nonuniformity of the voltage in both samples demonstrates that different charge carrier dynamics are taking place at the distinct CIGS grains. When the spatial variations in photovoltage of individual scans are compared (e.g., panels g and n of Figure 3), this behavior changes as a function of wavelength, demonstrating that the photovoltage signal results from the electrical response within the material (and not its surface only). Thus, through our imaging method we acquire a tomography of the electrical characteristics of the absorbing material where each scan corresponds to a snapshot of the mesoscale behavior of the grains composing the CIGS layer, as discussed later in this Letter. The word tomography is used here in the sense that we image the device in "sections" by illuminating it with different wavelength, which corresponds to a distinct penetration depth within the CIGS layer.

The spatial distribution of the voltage for each scan is used to quantify the occurrence of preferential charge carrier generation and collection sites as a function of wavelength and thus light penetration depth within the CIGS layer. As shown by the histograms in Figure 4, the voltage average value and distribution for each map vary as a function of wavelength. While the absorption coefficient is larger for shorter wavelengths (Figure S11), a smaller average value of the voltage is obtained. This behavior suggests that carriers generated near the top surface are more likely to recombine nonradiatively, leading to a smaller voltage. This observation is corroborated by the EQE data (Figure 1c), which also shows a decrease in carrier collection. For longer wavelengths, the absorption occurs deeper within the CIGS layer and leads to increased photovoltage until the bandgap is reached, where the voltage again decreases because of lack of photon absorption. The precise cause of the broadening of the voltage distribution with wavelength is unknown and is currently being investigated.

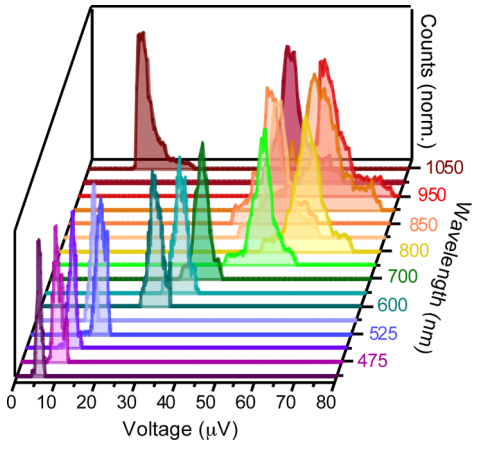

Figure 4. Three-dimensional plot of voltage histograms (normalized) as a function of wavelength for CIGS solar cell, obtained from scanning photovoltage microscopy (shown in Figure 3).

To further evaluate the spatial inhomogeneity of charge carrier dynamics within the CIGS layer, we analyze the voltage enhancement for the set of maps shown in Figure 3. Figure 5a shows a photovoltage scan acquired at 750 nm overlaid on the SEM image for the same 7 × 7 μm^2 region. Despite the fact that the scanning photovoltage measurements are limited by diffraction, notable spatial variations were consistently observed. Figure 5b displays the voltage enhancement as a function of wavelength for the positions (pixels) indicated by the colored circles in Figure 5a. Here, we define the enhancement as the voltage of a pixel, $V_{x,y}$, divided by the average value of the entire region, $\langle V \rangle$ (52.1 μV in this case). Note that both $V_{x,y}$ and $\langle V \rangle$ change for each incident wavelength (because of the CIGS absorption coefficient, see Figure S11). Surprisingly, some regions of the sample showed a modest voltage improvement of 10% for short wavelengths (400−500 nm) and a remarkable enhancement of 40% close to CIGS bandgap. The low electrical signal (black and cyan circles in Figure 5b) approaches the average value (green solid line) as the energy of the incident source of excitation nears the bandgap of CIGS. Interestingly, certain regions of the CIGS layer (red points in Figure 5b) present local voltage that varies 10% below and above the average response of the device, for wavelengths <550 nm and >600 nm, respectively. Near the material bandgap, the voltage enhancement reaches 20%. By spectrally and spatially resolving the photovoltage generated by the CIGS solar cell, we obtain a qualitative tomography of the local electrical characteristics of the device and probe their limiting factor: the V_{oc} (see Figure 5c). Here, the maps are displayed on the same voltage scale to emphasize the spatial variations as a function of the incident wavelength, which are likely due to the structural properties of the CIGS layer, instead of composition inhomogeneities between different grains. The longer-wavelength voltage maps do take into account the near-surface strong light absorption, and the qualitative tomography displays the contribution of the wavelength-dependent light absorption to the photovoltage.

Through a sequence of spectrally dependent photocurrent scans we determine the ΔV_{oc} map for the polished CIGS device under 1 sun illumination (Figure 6). This map is obtained by adding the contribution of each photocurrent scan to the overall short-circuit current map, $I_{sc,total}$, of the device, weighted by the number of photons incident into the sample at AM1.5G illumination, as

$$J_{sc,total} = \sum_{\lambda_n} J_{sc,\lambda_n}$$

$$J_{sc,\lambda_n} = I^{measured}_{sc,\lambda_n} \times \left[\int_{(\lambda+\lambda_{n-1})/2}^{(\lambda_{n+1}+\lambda)/2} \Phi_{1sun} \times \lambda \, d\lambda\right]/(P_{inc} \times \lambda_n)$$

DOI: 10.1021/acsenergylett.6b00331
ACS Energy Lett. 2016, 1, 899−905

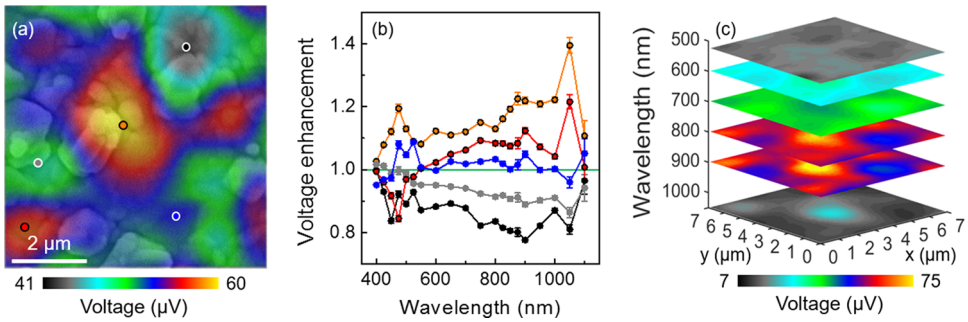

Figure 5. Mapping voltage with high spatial resolution in polycrystalline solar cells. (a) Voltage map overlaid with SEM image, acquired with wavelength λ = 750 ± 3 nm and incident power of 59 ± 1 nW. (b) Voltage enhancement as a function of wavelength (λ) for selected regions of the map shown in panel a. The green line corresponds to the average voltage value of each map, and the error bars refer to the standard deviation of each λ-dependent scan. (c) Qualitative tomography of photovoltage showing spatial variation as a function of λ. For each measurement, 100× objective lens (NA = 0.75).

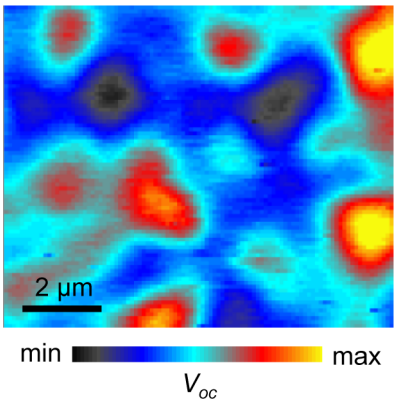

Figure 6. In situ characterization of the mesoscale behavior of CIGS solar cells. V_{oc} map for CIGS solar cell, with submicrometer spatial resolution, obtained from a sequence of spectrally dependent scans.

where J_{sc,λ_n} is the short-circuit current density for each wavelength λ_n where a scan was acquired, $I_{sc,\lambda_n}^{measured}$ the short-circuit current measured (a map), Φ_{1sun} the irradiance corresponding to 1 sun AM1.5G illumination (from Figure 3a), and P_{inc} the incident power for each measurement (wavelength dependent). Then, the V_{oc} map is determined by using the diode equation, where the ideality factor and the dark saturation current density (J_{dark}) were obtained from macroscopic measurements. The spatially resolved V_{oc} map combines the contribution of the surface and the bulk properties of the grains, weighted by the sun spectrum, mimicking the performance of a solar cell under realistic operation conditions. Although the polished sample has surface roughness of ∼100 nm (Figure S9), we were unable to acquire reliable information about the grains crystallographic orientation by EBSD because of the ZnO 500 nm layer (Figure 1a). Thus, the precise correlation between the spatial variations in V_{oc} and the structural properties of the CIGS requires the implementation of a selective chemical etching for removing the oxide layer. Nevertheless, this etching would necessarily be destructive and the exposure of the *n*-CdS would favor surface recombination, which directly affects the V_{oc} of the device.

Although microscopy methods such as KPFM[31,32] and EBIC[23,26] are more sensitive to measuring the local electrical response of solar cells, they are unlikely to become a portable tool for PV diagnosis. The conductive probe used in KPFM is very delicate and can easily lead to image artifacts, while EBIC requires an inert environment (vacuum). Furthermore, the electrical response of the device is extremely sensitive to the voltage of the electron beam. The quantitative analysis of the photovoltage requires combining the measurements with simulations of the interactions between the electron beam and the material. The spatial resolution of our diffraction-limited method could be improved by using near-field scanning optical microscopy probes as the source of illumination,[17] which can achieve resolution <100 nm. Nevertheless, the interpretation of the data in these cases often requires the consideration of near-field effects, and possibly the need for 3-dimensional simulations to help us understand the primary near-field light−matter interactions taking place. Here, we have implemented a universal, nondestructive imaging method to map the spatial variation of the electrical response of optoelectronic devices in situ that enabled a qualitative tomography of the generated photovoltage within the solar cell absorbing layer. Our functional characterization reveals how the electrical response of CIGS devices from a quaternary target changes spatially, considering light penetration depth. Furthermore, the submicrometer spatial resolution of the photovoltage scans presented here elucidates a pressing open question in the field of photovoltaics: *Does the V_{oc} of polycrystalline CIGS devices from a quaternary target vary spatially?* Yes.

In summary, we have demonstrated that the photovoltage of CIGS solar cells from a quaternary target varies locally by >20%, a behavior mapped for the first time here. We used micro-Raman imaging and EDX to determine the chemical composition of the grains. While the distribution of Cu, In, Ga, and Se was found to be uniform at the micrometer-scale, the V_{oc} of these devices is still considerably lower than expected. We implemented scanning photovoltage microscopy as an in situ functional characterization tool to resolve the local electrical response of CIGS, where we measured remarkable variations in voltage. A sequence of wavelength-dependent voltage scans enabled us to build a tomography of the photovoltage distribution within the CIGS layer, in which we demonstrated that some regions of the material outperform the average macroscopic behavior, potentially affecting the performance of the device. Finally, we presented a micrometer-scale resolved V_{oc} map under broadband illumination, revealing the spatial distribution of voltage for the CIGS solar cell under 1 sun global illumination operation conditions. Our functional imaging framework provides a novel tool for

DOI: 10.1021/acsenergylett.6b00331
ACS Energy Lett. 2016, 1, 899−905

mapping the electrical response of inhomogeneous materials for photovoltaics with micrometer-scale length grains, such as perovskites, CdTe, and CZTS. Furthermore, this nondestructive method can be expanded to other energy harvesting systems, such as perovskite solar cells, microstructured hot carrier devices, and photoelectrochemical cells.

■ ASSOCIATED CONTENT

Supporting Information

The Supporting Information is available free of charge on the ACS Publications website at DOI: 10.1021/acsenergylett.6b00331.

Experimental methods, schematic of experimental setup for photovoltage images, additional micro-Raman and photovoltage scans, and comparison between "as-is" and polished CIGS samples (PDF)

■ AUTHOR INFORMATION

Corresponding Author

*E-mail: mleite@umd.edu.

Author Contributions

M.S.L. conceived and directed the research. E.M.T. performed the macroscopic characterization and the micro-Raman and scanning photovoltage measurements. E.M.T., J.M.H., and W.B.G. calibrated the light source used in the photovoltage scans. J.A.F., J.D.M., and R.Y.B. designed and grew the CIGS samples. S.-M.N. performed the EBSD measurement. M.S.L. and E.M.T. analyzed the results and wrote the manuscript. All authors commented on the manuscript.

Funding

This project was funded through the University of Maryland Clark School of Engineering, the 2014 Minta Martin Award, the 2015 RASA Award, the 2015 Graduate School Summer Research Fellowship, and the 2016 Graduate Dean's Dissertation Fellowship.

Notes

The authors declare no competing financial interest.

■ ACKNOWLEDGMENTS

The authors acknowledge instrumentation assistance from E. Bailey, C. Gong, D. Ha, A. Flatau, M. Lumb, J. Murray, V. Nguyen, B. Sadowski, and J. Tischler; the technical assistance of the Maryland Nanocenter and WITec (Dr. W. Liu); and the critical reading of J. N. Munday. The financial support of the Clark School of Engineering, the 2014 Minta Martin Award, the 2015 RASA Award, the 2015 Graduate School Summer Research Fellowship, and the 2016 Graduate Dean's Dissertation Fellowship at the University of Maryland are greatly appreciated. The NRL authors gratefully acknowledge financial support from the Office of Naval Research and Sunlight Photonics, Inc.

■ REFERENCES

(1) Green, M. A. Commercial Progress and Challenges for Photovoltaics. *Nat. Energy* **2016**, *1*, 15015.

(2) Chirilă, A.; et al. Potassium-Induced Surface Modification of $Cu(In,Ga)Se_2$ Thin Films for High-Efficiency Solar Cells. *Nat. Mater.* **2013**, *12*, 1107−1111.

(3) Jackson, P.; Hariskos, D.; Wuerz, R.; Kiowski, O.; Bauer, A.; Friedlmeier, T. M.; Powalla, M. Properties of $Cu(In,Ga)Se_2$ Solar Cells with New Record Efficiencies up to 21.7%. *Phys. Status Solidi RRL* **2015**, *9*, 28−31.

(4) Green, M. A.; Emery, K.; Hishikawa, Y.; Warta, W.; Dunlop, E. D. Solar Cell Efficiency Tables (Version 48). *Prog. Photovoltaics* **2016**, *24*, 905−913.

(5) Liu, C.-H.; et al. Large Scale Single-Crystal $Cu(In,Ga)Se_2$ Nanotip Arrays For High Efficiency Solar Cell. *Nano Lett.* **2011**, *11*, 4443−4448.

(6) Harvey, T. B.; et al. Copper Indium Gallium Selenide (CIGS) Photovoltaic Devices Made Using Multistep Selenization of Nanocrystal Films. *ACS Appl. Mater. Interfaces* **2013**, *5*, 9134−9140.

(7) Frantz, J. A.; Bekele, R. Y.; Nguyen, V. Q.; Sanghera, J. S.; Bruce, A.; Frolov, S. V.; Cyrus, M.; Aggarwal, I. D. $Cu(In,Ga)Se_2$ Thin Films and Devices Sputtered from a Single Target without Additional Selenization. *Thin Solid Films* **2011**, *519*, 7763−7765.

(8) Shi, J. H.; Li, Z. Q.; Zhang, D. W.; Liu, Q. Q.; Sun, Z.; Huang, S. M. Fabrication of $Cu(In,Ga)Se_2$ Thin Films by Sputtering from a Single Quaternary Chalcogenide Target. *Prog. Photovoltaics* **2011**, *19*, 160−164.

(9) Ouyang, L.; Zhuang, D.; Zhao, M.; Zhang, N.; Li, X.; Guo, L.; Sun, R.; Cao, M. $Cu(In,Ga)Se_2$ Solar Cell with 16.7% Active-Area Efficiency Achieved by Sputtering from a Quaternary Target. *Phys. Status Solidi A* **2015**, *212*, 1774−1778.

(10) Dhere, N. G. Scale-up Issues of CIGS Thin Film PV Modules. *Sol. Energy Mater. Sol. Cells* **2011**, *95*, 277−280.

(11) Shockley, W.; Queisser, H. J. Detailed Balance Limit of p-n Junction Solar Cells. *J. Appl. Phys.* **1961**, *32*, 510.

(12) Nayak, P. K.; Bisquert, J.; Cahen, D. Assessing Possibilities and Limits for Solar Cells. *Adv. Mater.* **2011**, *23*, 2870−2876.

(13) Abou-Ras, D.; et al. Compositional and Electrical Properties of Line and Planar Defects in $Cu(In,Ga)Se_2$ Thin Films for Solar Cells. *Phys. Status Solidi RRL* **2016**, *10*, 363−375.

(14) Gorji, N. E. Degradation Sources of CdTe Thin Film PV: $CdCl_2$ Residue and Shunting Pinholes. *Appl. Phys. A: Mater. Sci. Process.* **2014**, *116*, 1347−1352.

(15) Durose, K.; et al. Physical Characterization of Thin-Film Solar Cells. *Prog. Photovoltaics* **2004**, *12*, 177−217.

(16) Kirchartz, T.; Rau, U. *Advanced Characterization Techniques for Thin Film Solar Cells*; Wiley-VCH: Weinheim, Germany, 2011; pp 1−547.

(17) Leite, M. S.; Abashin, M.; Lezec, H. J.; Gianfrancesco, A. G.; Talin, A. A.; Zhitenev, N. B. Nanoscale Imaging of Photocurrent and Efficiency in CdTe Solar Cells. *ACS Nano* **2014**, *8*, 11883−11890.

(18) Leite, M. S.; Abashin, M.; Lezec, H. J.; Gianfrancesco, A. G.; Talin, A. A.; Zhitenev, N. B. Mapping the Local Photoelectronic Properties of Polycrystalline Solar Cells Through High Resolution Laser-Beam-Induced Current Microscopy. *IEEE Journal of Photovoltaics* **2014**, *4*, 311−316.

(19) Bull, T. A.; Pingree, L. S. C.; Jenekhe, S. A.; Ginger, D. S.; Luscombe, C. K. The Role of Mesoscopic PCBM Crystallites in Solvent Vapor Annealed Copolymer Solar Cells. *ACS Nano* **2009**, *3*, 627−636.

(20) Ostrowski, D. P.; Glaz, M. S.; Goodfellow, B. W.; Akhavan, V. A.; Panthani, M. G.; Korgel, B. A.; Vanden Bout, D. A. Mapping Spatial Heterogeneity in $Cu(In_{1-x}Ga_x)Se_2$ Nanocrystal-Based Photovoltaics with Scanning Photocurrent and Fluorescence Microscopy. *Small* **2010**, *6*, 2832−2836.

(21) Howell, S. L.; Padalkar, S.; Yoon, K.; Li, Q.; Koleske, D. D.; Wierer, J. J.; Wang, G. T.; Lauhon, L. J. Spatial Mapping of Efficiency of GaN/InGaN Nanowire Array Solar Cells Using Scanning Photocurrent Microscopy. *Nano Lett.* **2013**, *13*, 5123−5128.

(22) Josell, D.; Debnath, R.; Ha, J. Y.; Guyer, J.; Sahiner, M. A.; Reehil, C. J.; Manners, W. A.; Nguyen, N. V. Windowless CdSe/CdTe Solar Cells with Differentiated Back Contacts: J−V, EQE, and Photocurrent Mapping. *ACS Appl. Mater. Interfaces* **2014**, *6*, 15972−15979.

(23) Moseley, J.; Metzger, W. K.; Moutinho, H. R.; Paudel, N.; Guthrey, H. L.; Yan, Y.; Ahrenkiel, R. K.; Al-Jassim, M. M. Recombination by Grain-Boundary Type in CdTe. *J. Appl. Phys.* **2015**, *118*, 025702.

DOI: 10.1021/acsenergylett.6b00331
ACS Energy Lett. 2016, 1, 899−905

(24) Nichterwitz, M.; Abou-Ras, D.; Sakurai, K.; Bundesmann, J.; Unold, T.; Scheer, R.; Schock, H. W. Influence of Grain Boundaries on Current Collection in Cu(In,Ga)Se_2 Thin-Film Solar Cells. *Thin Solid Films* **2009**, *517*, 2554−2557.
(25) Grabitz, P. O.; Rau, U.; Wille, B.; Bilger, G.; Werner, J. H. Spatial Inhomogeneities in Cu(In,Ga)Se_2 Solar Cells Analyzed by Electron Beam Induced Voltage Measurements. In *Conference Record of the 2006 IEEE 4th World Conference on Photovoltaic Energy Conversion*; 2006; pp 424−427. DOI: 10.1109/WCPEC.2006.279480.
(26) Yoon, H. P.; Haney, P. M.; Ruzmetov, D.; Xu, H.; Leite, M. S.; Hamadani, B. H.; Talin, A. A.; Zhitenev, N. B. Local Electrical Characterization of Cadmium Telluride Solar Cells Using Low-Energy Electron Beam. *Sol. Energy Mater. Sol. Cells* **2013**, *117*, 499−504.
(27) Kim, J.; Kim, S.; Jiang, C.-S.; Ramanathan, K.; Al-Jassim, M. M. Direct Imaging of Enhanced Current Collection on Grain Boundaries of Cu(In,Ga)Se_2 Solar Cells. *Appl. Phys. Lett.* **2014**, *104*, 063902.
(28) Azulay, D.; Millo, O.; Balberg, I.; Schock, H.-W.; Visoly-Fisher, I.; Cahen, D. Current Routes in Polycrystalline $CuInSe_2$ and Cu(In,Ga)Se_2 Films. *Sol. Energy Mater. Sol. Cells* **2007**, *91*, 85−90.
(29) Coffey, D. C.; Reid, O. G.; Rodovsky, D. B.; Bartholomew, G. P.; Ginger, D. S. Mapping Local Photocurrents in Polymer/Fullerene Solar Cells with Photoconductive Atomic Force Microscopy. *Nano Lett.* **2007**, *7*, 738−744.
(30) Kutes, Y.; Aguirre, B. A.; Bosse, J. L.; Cruz-Campa, J. L.; Zubia, D.; Huey, B. D. Mapping Photovoltaic Performance with Nanoscale Resolution. *Prog. Photovoltaics* **2016**, *24*, 315−325.
(31) Tennyson, E. M.; Garrett, J. L.; Frantz, J. A.; Myers, J. D.; Bekele, R. Y.; Sanghera, J. S.; Munday, J. N.; Leite, M. S. Nanoimaging of Open-Circuit Voltage in Photovoltaic Devices. *Adv. Energy Mater.* **2015**, *5*, 1501142.
(32) Dittrich, T.; Gonzales, A.; Rada, T.; Rissom, T.; Zillner, E.; Sadewasser, S.; Lux-Steiner, M. Comparative Study of Cu(In,Ga)Se_2/CdS and Cu(In,Ga)Se_2/In_2S_3 Systems by Surface Photovoltage Techniques. *Thin Solid Films* **2013**, *535*, 357−361.
(33) Tuteja, M.; Koirala, P.; MacLaren, S.; Collins, R.; Rockett, A. Direct Observation of Electrical Properties of Grain Boundaries in Sputter-Deposited CdTe Using Scan-Probe Microwave Reflectivity Based Capacitance Measurements. *Appl. Phys. Lett.* **2015**, *107*, 142106.
(34) McNeill, C. R.; Frohne, H.; Holdsworth, J. L.; Furst, J. E.; King, B. V.; Dastoor, P. C. Direct Photocurrent Mapping of Organic Solar Cells Using a Near-Field Scanning Optical Microscope. *Nano Lett.* **2004**, *4*, 219−223.
(35) Gütay, L.; Pomraenke, R.; Lienau, C.; Bauer, G. H. Subwavelength Inhomogeneities in Cu(In,Ga)Se_2 Thin Films Revealed by Near-Field Scanning Optical Microscopy. *Phys. Status Solidi A* **2009**, *206*, 1005−1008.
(36) Paetzold, U. W.; Lehnen, S.; Bittkau, K.; Rau, U.; Carius, R. Nanoscale Observation of Waveguide Modes Enhancing the Efficiency of Solar Cells. *Nano Lett.* **2014**, *14*, 6599−6605.
(37) Rau, U.; Taretto, K.; Siebentritt, S. Grain Boundaries in Cu(In,Ga) $(Se,S)_2$ Thin-Film Solar Cells. *Appl. Phys. A: Mater. Sci. Process.* **2009**, *96*, 221−234.
(38) Abou-Ras, D.; et al. Grain-Boundary Types in Chalcopyrite-Type Thin Films and Their Correlations with Film Texture and Electrical Properties. *Thin Solid Films* **2009**, *517*, 2545−2549.
(39) Bothe, K.; Bauer, G. H.; Unold, T. Spectrally Resolved Photoluminescence Studies on Cu(In,Ga)Se_2 Thin Films. *Thin Solid Films* **2002**, *403*−*404*, 453−456.
(40) Gütay, L.; Bauer, G. H. Spectrally Resolved Photoluminescence Studies on Cu(In,Ga)Se_2 Solar Cells with Lateral Submicron Resolution. *Thin Solid Films* **2007**, *515*, 6212−6216.
(41) Lombez, L.; Soro, M.; Delamarre, A.; Naghavi, N.; Barreau, N.; Lincot, D.; Guillemoles, J.-F. Revisiting the Interpretation of Biased luminescence: Effects on Cu(In,Ga)Se_2 Photovoltaic Heterostructures. *J. Appl. Phys.* **2014**, *116*, 064504.
(42) Bauer, G. H.; Brüggemann, R.; Tardon, S.; Vignoli, S.; Kniese, R. Quasi-Fermi Level Splitting and Identification of Recombination Losses from Room Temperature Luminescence in Cu(In_{1-x} Ga_x)Se_2 Thin Films Versus Optical Band Gap. *Thin Solid Films* **2005**, *480*−*481*, 410−414.
(43) Alberi, K.; Fluegel, B.; Moutinho, H.; Dhere, R. G.; Li, J. V.; Mascarenhas, A. Measuring Long-Range Carrier Diffusion across Multiple Grains in Polycrystalline Semiconductors by Photoluminescence Imaging. *Nat. Commun.* **2013**, *4*, 2699.
(44) Neumann, O.; Brüggemann, R.; Hariskos, D.; Witte, W.; Bauer, G. H. Photoluminescence Studies of Polycrystalline Cu(In,Ga)Se_2: Lateral Inhomogeneities Beyond Abbe's Diffraction Limit. *J. Appl. Phys.* **2015**, *118*, 185311.
(45) Li, C.; et al. Grain-Boundary-Enhanced Carrier Collection in CdTe Solar Cells. *Phys. Rev. Lett.* **2014**, *112*, 156103.
(46) Chakraborty, R.; Serdy, J.; West, B.; Stuckelberger, M.; Lai, B.; Maser, J.; Bertoni, M. I.; Culpepper, M. L.; Buonassisi, T. Development of an in-situ Temperature Stage for Synchrotron X-Ray Spectromicroscopy. *Rev. Sci. Instrum.* **2015**, *86*, 113705.
(47) Mainz, R.; et al. Annihilation of Structural Defects in Chalcogenide Absorber Films for High-Efficiency Solar Cells. *Energy Environ. Sci.* **2016**, *9*, 1818−1827.
(48) Xue, C.; Papadimitriou, D.; Raptis, Y. S.; Richter, W.; Esser, N.; Siebentritt, S.; Lux-Steiner, M. C. Micro-Raman Study of Orientation Effects of Cu_xSe-Crystallites on Cu-rich $CuGaSe_2$ Thin Films. *J. Appl. Phys.* **2004**, *96*, 1963−1966.
(49) Hsu, W.-C.; et al. Spatial Element Distribution Control in a Fully Solution-Processed Nanocrystals-Based 8.6% $Cu_2ZnSn(S,Se)_4$ Device. *ACS Nano* **2014**, *8*, 9164−9172.
(50) Luque, A.; Hegedus, S. *Handbook of Photovoltaic Science and Engineering*; John Wiley & Sons, Ltd: West Sussex, 2011.
(51) Fantoni, A.; Vieira, M.; Cruz, J.; Schwarz, R.; Martins, R. A Two-Dimensional Numerical Simulation of a Non-Uniformly Illuminated Amorphous Silicon Solar Cell. *J. Phys. D: Appl. Phys.* **1996**, *29*, 3154.
(52) Cuevas, A.; López-Romero, S. The Combined Effect of Non-Uniform Illumination and Series Resistance on the Open-Circuit Voltage of Solar Cells. *Sol. Cells* **1984**, *11*, 163−173.
(53) Nomura, S.; Ouchi, S.-i.; Endo, S. Raman Spectra of Ordered Vacancy Compounds in the Cu-In-Se System. *Jpn. J. Appl. Phys.* **1997**, *36*, L1075−L1077.
(54) Witte, W.; Kniese, R.; Powalla, M. Raman Investigations of Cu(In,Ga)Se_2 Thin Films with Various Copper Contents. *Thin Solid Films* **2008**, *517*, 867−869.
(55) Gloeckler, M.; Sites, J. R.; Metzger, W. K. Grain-Boundary Recombination in Cu(In,Ga)Se_2 Solar Cells. *J. Appl. Phys.* **2005**, *98*, 113704.
(56) Standard Tables for Reference Solar Spectral Irradiances: Direct Normal and Hemispherical on 37° Tilted Surface. ASTM International: West Conshohocken, PA, 2012. DOI: 10.1520/G0173-03R12.

DOI: 10.1021/acsenergylett.6b00331
ACS Energy Lett. 2016, 1, 899−905